A Data-Level Fusion Model for Developing Composite Health Indices for Degradation Modeling and Prognostic Analysis

Kaibo Liu, Nagi Z. Gebraeel, and Jianjun Shi

***Abstract*—Prognostics involves the effective utilization of condition or performance-based sensor signals to accurately estimate the remaining lifetime of partially degraded systems and components. The rapid development of sensor technology, has led to the use of multiple sensors to monitor the condition of an engineering system. It is therefore important to develop methodologies capable of integrating data from multiple sensors with the goal of improving the accuracy of predicting remaining lifetime. Although numerous efforts have focused on developing feature-level and decision-level fusion methodologies for prognostics, little research has targeted the development of "data-level" fusion models. In this paper, we present a methodology for constructing a composite health index for characterizing the performance of a system through the fusion of multiple degradation-based sensor data. This methodology includes data selection, data processing, and data fusion steps that lead to an improved degradation-based prognostic model. Our goal is that the composite health index provides a much better characterization of the condition of a system compared to relying solely on data from an individual sensor. Our methodology was evaluated through a case study involving a degradation dataset of an aircraft gas turbine engine that was generated by the Commercial Modular Aero-Propulsion System Simulation (C-MAPSS).**

***Note to Practitioners*—The advancement in sensor technology facilitates vigorous development in multisensor systems, which have been widely used to monitor the degradation status of each system or unit. In order to improve the remaining life prediction, data fusion techniques have been developed based on feature-level and decision-level fusions. This paper presents a new approach that is based on the data-level fusion technique to construct a health index for degradation modeling and prognostics. The proposed methodology is especially beneficial for the cases where degradation occurs in a cumulative manner under a single operation condition, which results from a single failure mode. To implement this methodology, it is necessary: 1) to identify the physical system associated with the degradation process; 2) to collect sample degradation signals from multiple sensors; 3) to screen out useful sensor data by data processing and sensor selection step; and 4) to train the optimal weights on the basis of two essential properties of degradation signals. Once the optimal weights are obtained in the training stage, the health index can be developed for degradation modeling and prognostics in the testing stage. One advantage of this proposed methodology is that it does not conflict with other feature-level or decision-level fusion approaches, which can still be implemented to further improve remaining life prediction by treating the composite health index as another sensor data. Experimental studies show that the composite health index has better performance than any other original sensor information when it is used for model fitting and remaining life prediction. The methodology developed in this paper can lead to a great impact on data-driven degradation modeling and prognostics. In future research, we will extend our work to the cases that have more than one failure mode and operation condition. In addition, we will investigate the extensions of this proposed methodology by using kernel methods to map the *in-situ* sensor data into higher dimensional space.**

***Index Terms*—Data-level fusion, degradation modeling, prognostics, residual life distributions.**

Manuscript received May 27, 2012; revised October 12, 2012; accepted February 20, 2013. Date of publication April 11, 2013; date of current version June 27, 2013. This paper was recommended for publication by Associate Editor Q. Huang and Editor L. Shi upon evaluation of the reviewers' comments. This work was supported by the National Science Foundation (NSF) under Grant CMMI-0738647 and Grant CMMI-0927574. *(Corresponding author: J. Shi.)*

The authors are with the H. Milton Stewart School of Industrial and Systems Engineering, Georgia Institute of Technology, Atlanta, GA 30332 USA (e-mail: kbliu@gatech.edu; nagi@isye.gatech.edu; jianjun.shi@isye.gatech.edu).

Digital Object Identifier 10.1109/TASE.2013.2250282

NOMENCLATURE

$x_{i,k,j}$	the sensor measurement for unit i, sensor k and observation epoch j;
$b_{i,j}$	the composite health index for unit i and observation epoch j;
n_i	the number of available observation epochs for unit i;
m	the total number of training units;
s	the number of selected sensors for data-level fusion;
$\varepsilon_{i,j}$	the slack variable that measures the amount of violation in the monotonic property of the composite health index for unit i and observation epoch j;
$c_{i,j}$	the weight coefficient corresponding to the slack variable $\varepsilon_{i,j}$;
r	the tuning parameter that controls the relative importance of two terms, the amount of violation in monotonicity and the variance in the failure threshold of the composite health index;
r^*	the optimal value of r;
t_f	the incipient fault time when fault occurs;
$\tilde{t}_f^i$	the estimated incipient fault time for unit i;
q	the common ratio when $\{c_{i,j}\}$ is a geometric series;
p	the constant number that represents the number of observation epochs taken into consideration for data-fusion algorithm;

VM_k, VF_k the amount of violation in the monotonic property and the variance in the failure threshold in the kth cross-validation;

VM, VF the average amount of violation in the monotonic property and the average variance in the failure threshold by K-fold cross-validation;

ϕ_k the constant parameter in the exponential functional form when fitting $x_{i,k,j}$;

$\theta_{i,k}, \alpha_{i,k}, \beta_{i,k}$ the random variables in the exponential functional form when fitting $x_{i,k,j}$;

$\theta'_{i,k}$ the random variable in the exponential functional form when fitting L_{i,k,n_i+t};

$\tau_{i,k}(j)$ the normally distributed random error term in the exponential functional form when fitting $x_{i,k,j}$;

σ_k^2 the variance of the random error term $\tau_{i,k}(j)$;

$\tilde{T}_{i,k}$ the estimated remaining lifetime for unit i based on sensor k;

T_i the actual remaining lifetime for unit i;

$L_{i,k,j}$ the data after log transformation of $x_{i,k,j}$;

$\tilde{u}_{i,k,n_i+t}$ the mean of the log transformed data L_{i,k,n_i+t};

$\tilde{\sigma}^2_{i,k,n_i+t}$ the variance of the log transformed data L_{i,k,n_i+t};

u_d^k, v_d^k the mean and the variance of failure threshold for sensor k;

$F_{\tilde{T}_{i,k}|\boldsymbol{L}_{\boldsymbol{i},\boldsymbol{k},.}}(t)$ the conditional cumulative distribution function (cdf) of the estimated remaining lifetime $\tilde{T}_{i,k}$ given the historical data $\boldsymbol{L}_{\boldsymbol{i},\boldsymbol{k},.}$;

$\mathrm{err}_{i,k}$ the percentage error that measures the relative difference between the predicted and the actual failure time for unit i and sensor k;

$\boldsymbol{w}$ the vector of weight coefficients to combine multiple sensor data;

$\boldsymbol{w}^*$ the optimal vector of $\boldsymbol{w}$;

$\boldsymbol{\omega_i}$ the vector of variables to maximizing the monotonic property for unit i;

$\boldsymbol{\varepsilon_{i,.}}$ the vector of slack variables for unit i;

$\boldsymbol{c_{i,.}}$ the vector of weight coefficients corresponding to $\boldsymbol{\varepsilon_{i,.}}$ for unit i;

$\boldsymbol{\omega}$ the vector of variables that consist of $\boldsymbol{w}$ and all slack variables;

$\boldsymbol{\omega}^*$ the optimal vector of $\boldsymbol{\omega}$;

$\boldsymbol{l}$ the vector of weights for the selected sensors and all slack variables;

$\boldsymbol{\Gamma_{i,k}}$ the vector of jointly distributed stochastic parameters $\theta'_{i,k}$, $\alpha_{i,k}$ and $\beta_{i,k}$;

$\boldsymbol{u_0^k}, \boldsymbol{u_p^{i,k}}$ the prior and the posterior mean of $\boldsymbol{\Gamma_{i,k}}$;

$\boldsymbol{L_{i,k,.}}$ the vector of the log transformed data observed up to current observation epoch n_i for unit i and sensor k;

$\boldsymbol{L_{.,k,n_.}}$ the vector of the log transformed data that record the last observations before failure in all training units for sensor k;

$\boldsymbol{Y}$ the matrix that records the last observations before failure with the rows corresponding to each training unit and the columns corresponding to each selected sensor;

$\boldsymbol{D}$ the constant symmetric matrix used to calculate the variance in the failure threshold;

$\boldsymbol{M}$ the diagonal matrix with 1 (-1) on the diagonal entry if the corresponding sensor information shows an increasing (a decreasing) trend;

$\boldsymbol{E_i}$ the matrix constructed by the selected sensor data and identity matrix to maximize the monotonic property for unit i;

$\boldsymbol{Z}^{a\times b}$ the a-by-b matrix with all-zero entries;

$\boldsymbol{O}$ the matrix with all-one entries;

$\boldsymbol{G}$ the constant matrix constructed by identity matrix and $\boldsymbol{Z}^{s\times(\sum_{i=1}^{m}(n_i-1))}$;

$\boldsymbol{N}$ the matrix constructed by $\boldsymbol{M}$ and $\boldsymbol{Z}^{s\times(\sum_{i=1}^{m}(n_i-1))}$;

$\boldsymbol{A_i}$ the matrix constructed by the selected sensor data to maximize the monotonic property for unit i;

$\boldsymbol{A}$ the matrix constructed by all $\boldsymbol{A_i}$;

$\boldsymbol{I}$ the identity matrix;

$\boldsymbol{F}$ the matrix constructed by $\boldsymbol{M}, \boldsymbol{A}, \boldsymbol{Z}^{s\times(\sum_{i=1}^{m}(n_i-1))}$ $\boldsymbol{Z}^{(\sum_{i=1}^{m}(n_i-1))\times s}$ and identity matrix;

$\boldsymbol{H}$ the matrix constructed by $\boldsymbol{G}, \boldsymbol{y}$ and $\boldsymbol{D}$;

$\boldsymbol{\Sigma_0^k}, \boldsymbol{\Sigma_p^{i,k}}$ the prior and the posterior variance of $\boldsymbol{\Gamma_{i,k}}$;

$\boldsymbol{\Psi_i}$ the matrix associated with the vector $\boldsymbol{\Gamma_{i,k}}$ to calculate the fitted value for the log transformed data up to observation epoch n_i;

For consistency, we use bold face style for vectors and matrices. All matrices are written in capital letter whereas vectors are written in lowercase. All vectors are assumed to be column vectors.

I. Introduction

UNEXPECTED equipment failure often lead to severe economic losses and can sometimes have catastrophic consequences. A typical example that occurs in the industrial sector is unexpected machine failures that result in production

downtime, delayed delivery schedule, poor customer satisfaction, and safety issues. Condition monitoring and prognostics, which utilize sensor data to assess the health status of equipment and make inferences about the remaining lifetime, play important roles in condition-based maintenance [1]. As equipment degrade, sensor data related to the underlying failure processes (such as temperature, vibration, emissions, etc.) evolve in a manner that is related to the severity of degradation process and are typically referred to as degradation signals. Given a predetermined failure threshold, monitoring these degradation signals can provide accurate inferences about the remaining lifetime of each system or unit.

The literature pertaining to modeling degradation processes is indeed rich, and contains numerous methods and techniques [2], [3]. However, most of the existing models study only a single measure for degradation. These approaches are effective when the degradation mechanism is well understood and a single sensor is capable of capturing most of the characteristics of the underlying degradation process. In reality, a single sensor is typically insufficient for characterizing various types of manifestations that may result from even a single degradation process. Although it is possible to use multiple sensors and individually analyze the corresponding data, this can often result in significant over or under estimation of the remaining lifetime [4]. In fact, different sensor data may exhibit different signal patterns. Some sensors are highly related to the degradation mechanism, and thus can show a strong degradation trend while others may not. Two key challenges when performing prognostics using multiple sensors are: 1) deciding on which specific sensor data to use for modeling degradation and 2) how to combine/fuse multiple relevant sensor data. Generally, data collected from multiple sensors may contain only partial information about the same degradation process, and thus fusing this information has the potential to provide more accurate and robust prognostic capability. In addition, the data fusion approach can save cost by identifying and collecting only relevant sensor data for prognostics in future monitoring.

There are three categories of data fusion that are classified based on the level of implementation of the fusion methodology: data-level fusion, feature-level fusion, and decision-level fusion [5], [6]. Data-level fusion combines multiple sensor data that measure correlated parameters. Heger and Pandit [7] applied a data-level fusion approach by using multidirectional illumination and image fusion to generate an image with a high degree of relevant information for grinding tool condition monitoring and fault diagnostic applications. Kalman filter is another common technique applied to multisensor fusion [8], [9]. Salahshoor *et al.* [10] presented an integrated design framework based on the extended Kalman filter (EKF) data fusion algorithm for enhancing the detection and diagnosis of sensor and process faults. On the other hand, feature-level fusion integrates feature information that results from independent analysis methods. Prior knowledge about the degradation mechanism and physical laws are usually implemented to create desired features. For example, Goebel and Bonissone [11] applied a feature-level fusion approach to predict industrial web paper breakage using an Adaptive Neuro-Fuzzy Inference System (ANFIS) model. Volponi *et al.* [6] performed information fusion at the feature-level to maximize the amount of meaningful information that can be extracted from separate data sources to obtain comprehensive diagnostic and prognostic knowledge regarding the health of the aircraft gas turbine engine. Finally, decision-level fusion involves integrating diagnostic actions (e.g., preliminary determination of an entity's location, attributes, and identity). Sun [12] conducted a decision-level fusion analysis for vehicle health monitoring and degradation detection where decisions were made based on each sensor and their features (e.g., power spectrum, wavelets, AR modeling, and entropy spectrum). A review of some of the literature on multisensor data fusion approaches to condition monitoring, fault diagnosis, and prognostics can be found in Jardine *et al.* [13].

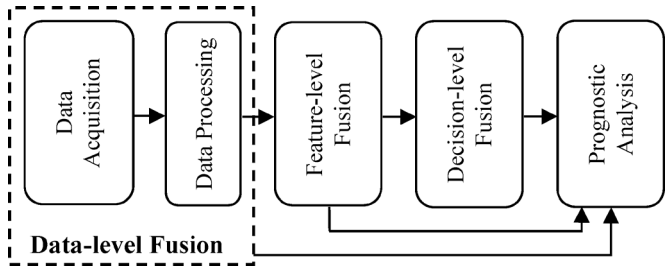

Fig. 1. Different levels of data fusion approaches to prognostic analysis.

While the aforementioned techniques were effective in different levels of data fusion, most of them aimed at improving monitoring and diagnostic performances. Little literature has discussed how these methodologies can be applied to degradation modeling and prognostics. Some extensions to prognostic applications can be found in feature-level and decision-level fusion models [14], [15], but seldom at data-level fusion. One possible explanation is that feature-level and decision-level fusion models are performed on intermediate results, i.e., after analyzing the original data. In such scenarios, it is usually more flexible to aggregate the information from independent analysis techniques (feature-level) or decisions (decision-level). Nonetheless, these two approaches are highly dependent on the quality of the raw data, and how that data is analyzed and processed. Therefore, there is a significant need to develop a data-level fusion technique that deals with constructing an efficient composite health index that is specific and relevant to degradation modeling and prognostics. This composite health index can be regarded as the key metric for assessing the health status of each unit. Feature-level and decision-level fusion techniques can still be implemented on the basis of the constructed health index to further improve prognostic results. Fig. 1 illustrates a flow chart on different levels of data fusion approaches to final prognostic analysis. The contribution of this paper is highlighted by the dashed rectangle in Fig. 1.

The remainder of this paper is organized as follows. Section II describes the simulation model developed using the NASA Commercial Modular Aero-Propulsion System Simulation (C-MAPSS) for commercial aircraft gas turbine engines, and provides an overview of the degradation dataset taken from Saxena *et al.* [16]. Section III develops a concrete formulation of constructing an efficient composite health index based on the data-level fusion technique for degradation modeling and prognostics. Key elements related to the problem formulation,

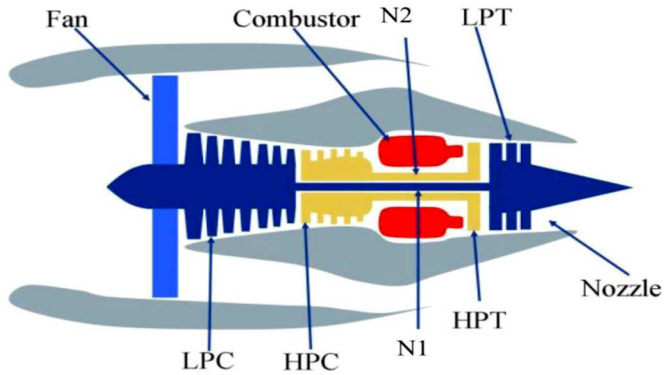

Fig. 2. Simplified engine diagram simulated in C-MAPSS [18].

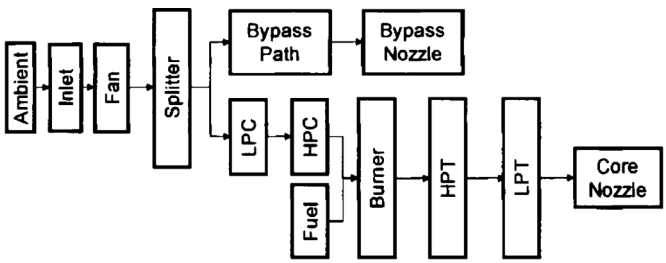

Fig. 3. A layout of modules and connections in the simulation [18].

which include essential properties for developing degradation signals, algorithm robustness, weight coefficients setting, selection of data-fusion function, and tuning parameter setting, will be addressed. Section IV demonstrates the improved performance of the composite health index when it is used for model fitting and remaining life prediction based on the dataset introduced in Section II. Section V draws a conclusion and discusses future research directions.

II. Overview of the System and Dataset

A. System Model Description

This paper considers the degradation of a simulated turbofan engine that is monitored using multiple sensors. The simulation model of the turbofan engine was developed using C-MAPSS, a simulation tool developed at NASA and widely used in engine health monitoring research for simulating realistic large commercial turbofan engines [16], [17]. Fig. 2 provides a schematic diagram of a commercial aircraft gas turbine engine that was simulated using C-MAPSS. Fig. 3 presents the main subroutines used in the simulation model.

A model of a 90 000 lb thrust engine is developed and simulations are run for operations at altitude from 0 to 42 000 ft., Mach number (speed) from 0 to 0.84, and throttle resolver angle (TRA) from 20 to 100. Users can adjust these three conditions: aircraft altitude, Mach number (speed), and TRA to simulate different environmental conditions. The C-MAPSS simulation model is embedded in a MATLAB Simulink platform. The software allows running in a closed-loop environment, and thus no user input is required during replications. The software has 14 inputs and can generate 21 outputs that are available for analysis. Those 21 outputs are described in Table I.

TABLE I
Sensors With Available Data [16]

Symbol	Description	Units
T2	Total temperature at fan inlet	°R
T24	Total temperature at LPC outlet	°R
T30	Total temperature at HPC outlet	°R
T50	Total temperature at LPT outlet	°R
P2	Pressure at fan inlet	psia
P15	Total pressure in bypass-duct	psia
P30	Total pressure at HPC outlet	psia
Nf	Physical fan speed	rpm
Nc	Physical core speed	rpm
epr	Engine pressure ratio (P50/P2)	--
Ps30	Static pressure at HPC outlet	psia
phi	Ratio of fuel flow to Ps30	pps/psi
NRf	Corrected fan speed	rpm
NRc	Corrected core speed	rpm
BPR	Bypass Ratio	--
farB	Burner fuel-air ratio	--
htBleed	Bleed Enthalpy	--
Nf_dmd	Demanded fan speed	rpm
PCNfR_dmd	Demanded corrected fan speed	rpm
W31	HPT coolant bleed	lbm/s
W32	LPT coolant bleed	lbm/s

The basis for developing the simulation model was that damage accumulation will be different for each engine, and thus will not be directly quantifiable based on the flight duration and flight conditions. Consequently, the underlying assumption was users had to rely on sensor data collected during each flight to make decisions regarding the health state of the engine. The simulation model was specifically used to characterize degradation in engine performance due to wear and tear based on the usage pattern of the engines. In order to make it more realistic, an unknown variance in the initial level of wear and random noise were introduced to represent system variability. In other words, each engine started with different degrees of initial wear and manufacturing variation, which was unknown to the user until the failure threshold was reached. The failure threshold was used to define the end-of-life (EoL) beyond which the unit is considered to have failed. Note that users did not have explicit access to the simulation model and the failure threshold was not announced a priori. A detailed description of the process by which the data was generated is discussed in [16].

B. Dataset Description

A total of four datasets were generated using this simulation model along with the corresponding failure mode and operational conditions [16]. In this paper, we consider the data pertaining to a single failure mode and a single operating condition. However, our approach can be extended to scenarios with multiple failure modes and multiple operating conditions in future studies. The dataset considered in this work consists of 100 training units, 100 testing units, and a file recording the actual remaining lifetime of the 100 testing units. Each training unit is run to failure, while each testing unit is stopped at some random point prior to its failure. Time is measured in observation epochs, in this case, number of flights. Sensor readings from the 21 outputs are collected after each observation epoch for each unit.

III. Development of a Degradation Data-Level Fusion Methodology

We develop a data-level fusion methodology for combining degradation signals from multiple sensors with the objective of constructing a composite health index that accurately characterizes the underlying degradation process and can be used to perform precise prognostic analysis. One critical challenge is how to guarantee that the resulting composite health index is more suitable for degradation modeling and prognostics than any one of the original sensor signal. To answer this question, we first define a few essential properties that if present in a degradation signal, can enhance its effectiveness when used for prognostics.

A. Essential Properties for Developing Degradation Signals

Saxena *et al.* [19] pointed out the inconsistencies in the choice of metrics when comparing the performance of various prognostic techniques, and further summarized and suggested several general metrics that can be used for prognostic applications. Although the efforts in [19] focused on proposing metrics for evaluating performance of prognostic techniques instead of degradation signals, the authors indicated some desirable properties that degradation signals should have for successful prognostic applications.

Property 1: Once an initial fault occurs, the trend of the degradation signals should be monotonic.

Property 2: Given the same environmental conditions and failure modes, the variance in the failure threshold of different units should be minimal.

Property "1" suggests that although raw sensor data may be nonmonotonic due to noise, it is important to develop a composite health index that has a clearer monotonic trend. On the other hand, property "2" implies that for a given raw sensor data, there may be significant differences among the failure threshold of different units. However, it is important to develop a composite health index that has the least possible variation in its failure threshold. Since we assume that each engine fails due to a single failure mode under a single operating condition, we expect that a composite health index that exhibits a consistent pattern for all units as engine degrades, which can be achieved by jointly maximizing the monotonic property and minimizing the variance in the failure threshold when constructing the health index.

B. Problem Formulation

Using these two properties, we formulate our data-level fusion methodology as a quadratic programming problem

$$\begin{aligned}\text{obj} =& \min_{\boldsymbol{w},\varepsilon_{i,j}} (1-r)\sum_{i=1}^{m}\sum_{j=1}^{n_i-1} c_{i,j}\varepsilon_{i,j} \\ &+ r\boldsymbol{w}'\boldsymbol{Y}'\boldsymbol{D}\boldsymbol{Y}\boldsymbol{w}, \\ &\text{s.t. } \boldsymbol{w}'\boldsymbol{M}'\boldsymbol{1} = 1, \quad \boldsymbol{M}\boldsymbol{w} \geq \boldsymbol{0}, \quad \boldsymbol{E_i}\boldsymbol{\omega_i} \geq \boldsymbol{0}, \\ &\varepsilon_{i,j} \geq 0, i = 1, \quad \ldots, m, \quad j = 1, \ldots, n_i - 1 \end{aligned} \tag{1}$$

where $\varepsilon_{i,j}$ is the slack variable that measures the amount of violation in monotonicity of the composite health index for unit i and observation epoch j; $c_{i,j}$ is a weight coefficient for the slack variable $\varepsilon_{i,j}$; n_i is the number of available observation epochs in each unit i; m is the total number of training units; $\boldsymbol{w} \in R^{s\times 1}$ is the vector of weight coefficients used to combine multiple sensor data at each observation epoch for each unit, where s is the number of selected sensors;$\boldsymbol{Y} \in R^{m\times s}$ is the matrix recording the last observations before failure with the rows representing each training unit and the columns representing each selected sensor; $\boldsymbol{D} \in R^{m\times s}$ is a symmetric matrix of following form: $\boldsymbol{D} = (\boldsymbol{I} - \boldsymbol{O}/m)/(m-1)$, where $\boldsymbol{O}$ is a matrix of all ones and $\boldsymbol{I}$ is an identity matrix; $\boldsymbol{M} \in R^{s\times s}$ is a diagonal matrix denoting the degradation trend information with 1 (-1) on the diagonal entry if the corresponding sensor information shows an increasing (decreasing) trend; $\boldsymbol{\omega_i} = [\boldsymbol{w}', \varepsilon_{i,1}, \ldots, \varepsilon_{i,n_i-1}]' \in R^{(s+n_i-1)\times 1}$ is a vector that needs to be determined for unit i such that the composite health index for unit i remains monotonic after adding the slack variables $\varepsilon_{i,1}, \ldots, \varepsilon_{i,n_i-1}$ at each observation epoch; $\boldsymbol{E_i} \in R^{(n_i-1)\times(s+n_i-1)}$ is the matrix used to maximize the monotonicity for unit i and has the following form:

$$\boldsymbol{E_i} = \begin{bmatrix} x_{i,1,2} - x_{i,1,1} & \cdots & x_{i,s,2} - x_{i,s,1} & \\ \cdots & \cdots & \cdots & \boldsymbol{I} \\ x_{i,1,n_i} - x_{i,1,n_i-1} & \cdots & x_{i,s,n_i} - x_{i,s,n_i-1} & \end{bmatrix}$$

where $x_{i,k,j}$ is the sensor data for unit i, sensor k and observation epoch j; r is a tuning parameter controlling the relative importance of these two additive terms in the quadratic formulation. Discussions on determining the values of c_{ij} and $\boldsymbol{M}$ can be found in the next subsection.

The formulation in (1) is inspired by the modeling efforts in linear support vector machines (SVM) for nonseparable case [20]. The main idea of SVM is to select a hyperplane that creates the biggest margin between the training points for two different classes. In the case that a point is classified on the wrong side of the margin, which is called nonseparable case of SVM, a slack variable is introduced to measure the distance of this point to the correct side of the margin. Similarly, the slack variable $\varepsilon_{i,j}$ is added in (1) to compensate for the violation in monotonicity. Thus, if we denote the composite health index for unit i and observation epoch j as $b_{i,j}$, then, $\varepsilon_{i,j} = \max(b_{i,j} - b_{i,j+1}, 0)$ when solving (1).

The objective function in (1) is the summation of two parts: $\sum_{i=1}^{m}\sum_{j=1}^{n_i-1} c_{i,j}\varepsilon_{i,j}$ measures the total weighted amount of violation in monotonicity for Property "1" and $\boldsymbol{w}'\boldsymbol{Y}'\boldsymbol{D}\boldsymbol{Y}\boldsymbol{w}$ measures the variance in the failure threshold for Property "2" (see Appendix A for details). Therefore, (1) reflects a tradeoff between maximizing the monotonic property and minimizing the variance in the failure threshold for prognostics.

To facilitate solving this optimization model, the formulation expressed in (1) can be simplified as follows:

$$\begin{aligned}\text{obj} =& \min_{\boldsymbol{\omega}} (1-r)\boldsymbol{l}'\boldsymbol{\omega} + r\boldsymbol{\omega}'\boldsymbol{H}\boldsymbol{\omega} \\ &\text{s.t. } \boldsymbol{\omega}'\boldsymbol{N}'\boldsymbol{1} = 1, \boldsymbol{F}\boldsymbol{\omega} \geq \boldsymbol{0} \end{aligned} \tag{2}$$

where $\boldsymbol{l} \in R^{(s+\sum_{i=1}^{m}(n_i-1))\times 1}$ is the vector of weights for the selected sensors and all slack variables, and equals to $[\boldsymbol{Z}^{1\times s}, \boldsymbol{c}'_{\boldsymbol{1},.}, \ldots, \boldsymbol{c}'_{\boldsymbol{m},.}]'$, where the matrix $\boldsymbol{Z}^{a\times b}$ is an a-by-b matrix with all zero entries and $\boldsymbol{c_{i,.}} = [c_{i,1}, \ldots, c_{i,n_i-1}]'$; $\boldsymbol{H} = \boldsymbol{G}'\boldsymbol{Y}'\boldsymbol{D}\boldsymbol{Y}\boldsymbol{G}$, where $\boldsymbol{G} \in R^{s\times(s+\sum_{i=1}^{m}(n_i-1))}$ and equals to $[\boldsymbol{I} \ \boldsymbol{Z}^{s\times(\sum_{i=1}^{m}(n_i-1))}]$. Note that $\boldsymbol{D}$ is a positive semidefinite (P.S.D) matrix, and therefore it can be

shown that $\boldsymbol{H}$ is also P.S.D. (see Appendix B for details). Thus, a global minimizer exists in (2) as long as there is a feasible vector $\boldsymbol{\omega} \in R^{(s+\sum_{i=1}^{m}(n_i-1))\times 1}$, where $\boldsymbol{\omega} = [\boldsymbol{w}', \boldsymbol{\varepsilon}'_{1,.}, \ldots, \boldsymbol{\varepsilon}'_{\boldsymbol{m},.}]'$ and $\boldsymbol{\varepsilon}_{\boldsymbol{i},.} = [\varepsilon_{i,1}, \ldots, \varepsilon_{i,n_i-1}]'$. Finally, $\boldsymbol{N} \in R^{s\times(s+\sum_{i=1}^{m}(n_i-1))}$ and is equal to $[\boldsymbol{M}\ \boldsymbol{Z}^{s\times(\sum_{i=1}^{m}(n_i-1))}]$; $\boldsymbol{F} \in R^{(s+2*\sum_{i=1}^{m}(n_i-1))\times(s+\sum_{i=1}^{m}(n_i-1))}$ and has the following form:

$$\boldsymbol{F} = \begin{bmatrix} \boldsymbol{M} & \boldsymbol{Z}^{s\times(\sum_{i=1}^{m}(n_i-1))} \\ \boldsymbol{A} & \boldsymbol{I} \\ \boldsymbol{Z}^{(\sum_{i=1}^{m}(n_i-1))\times s} & \boldsymbol{I} \end{bmatrix}$$

where $\boldsymbol{A} \in R^{(\sum_{i=1}^{m}(n_i-1))\times s}$ and

$$\boldsymbol{A} = \begin{bmatrix} \boldsymbol{A_1} \\ \ldots \\ \boldsymbol{A_m} \end{bmatrix}; \quad \boldsymbol{A_i} \in R^{(n_i-1)\times s}$$

and

$$\boldsymbol{A_i} = \begin{bmatrix} x_{i,1,2} - x_{i,1,1} & \ldots & x_{i,s,2} - x_{i,s,1} \\ \ldots & \ldots & \ldots \\ x_{i,1,n_i} - x_{i,1,n_i-1} & \ldots & x_{i,s,n_i} - x_{i,s,n_i-1} \end{bmatrix}.$$

C. Model Settings and Parameter Selections

In this section, we discuss several key elements related to our model formulation. Specifically, we focus on data processing and sensor selection, algorithm robustness, setting weight coefficients for $c_{i,j}$, selection of data-fusion function, and tuning parameter setting.

1) Data Processing and Sensor Selection: Since multiple sensors are observed during operation, the first step is to determine which of these sensors should be selected as input to our data-level fusion model. As a preliminary criterion, we focus on sensors that generate signals that exhibit a characteristically increasing or decreasing trend. Thus, we will select a sensor if its last observation is relatively larger (increasing trend) or smaller (decreasing trend) than the initial observation for all the training units. Once the sensors have been selected and trend information has been identified, then s and $\boldsymbol{M}$ can be determined. Without loss of generality, all sensor data will be standardized.

2) Algorithm Robustness: In many applications, sensor signals may exhibit a relatively stationary trend associated with the nondefective phase of a unit's operation. This may be followed by a defective phase where a unit is still operational but its degradation gradually worsens over time. This phenomenon can be reflected in the characteristics of the degradation signal. For example, in [21], the authors identified two distinct phases for bearing applications. The first phase was referred to as the nondefective phase and extended from the point of new equipment installation until the very first onset of a fault. In this work, we refer to the time corresponding to the initial fault as the incipient fault time, which we denote as t_f. The second phase was referred to the defective phase. It started from the time of the incipient fault t_f and extended until the point of failure, i.e., when the signal crossed the designated failure threshold.

The dataset used in this paper also exhibits similar characteristics. For example, Fig. 4 illustrates these two phases

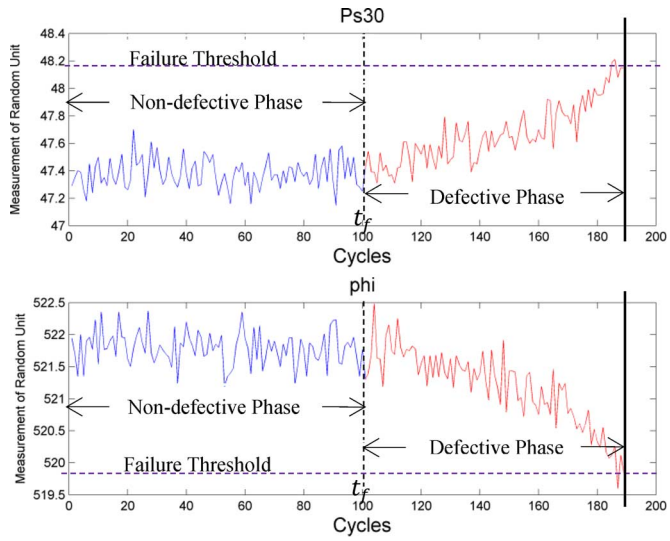

Fig. 4. Illustration of two phases in degradation signals.

in the degradation signals observed from two sensors "Ps30" and "phi." A vertical dashed line is used to distinguish these two phases. The horizontal dashed line is used to represent the respective failure thresholds. Since no degradation occurs in the nondefective phase, the sensor data observed during that phase does not show a significant trend. Consequently, from a prognostics perspective, it cannot be used to predict remaining lifetime. Thus, only the sensor data pertaining to the defective phase should be used to develop our composite health index. Specifically, we may replace the term $\sum_{i=1}^{m}\sum_{j=1}^{n_i-1} c_{i,j}\varepsilon_{i,j}$ with $\sum_{i=1}^{m}\sum_{j=\tilde{t}_f^i}^{n_i-1} c_{i,j}\varepsilon_{i,j}$ in (1), where $\tilde{t}_f^i$ is the estimated incipient fault time for unit i.

The key challenge now will be to automatically identify the incipient fault time. Detection of incipient faults for automatic inspection and minimization of maintenance costs has been studied extensively [22]. One approach is to build a time series model with moving time windows for each training unit. A CUSUM or exponentially weighted moving average (EWMA) control chart can then be used to monitor the changes in the model residuals [23]. Although some efforts have been made [24]–[26], in numerous applications, the accurate identification of incipient fault time using *in-situ* sensor data is still an ongoing research area. In this paper, we focus on how to assign the weight coefficients $c_{i,j}$ such that the resulting health index is robust with respect to the uncertainties in estimating the incipient fault time.

3) Setting Weight Coefficients: Recall that $\boldsymbol{\varepsilon_i}_{,.}$ measures the amount of violation in monotonicity as unit i degrades, and $\boldsymbol{c'_{i,.}}\boldsymbol{\varepsilon_i}_{,.}$ is the total weighted sum of violations in monotonicity for unit i. As a unit degrades, the accuracy of predicting its remaining lifetime becomes increasingly sensitive to the amount of violations in monotonicity of the degradation signal. Therefore, we assign higher weights to the slack variables, $\varepsilon_{i,j}$ (see (1)), as j increases, where j is the observation epoch. Consequently, we define the following condition for $c_{i,j}$:

$$c_{i,j+1} \geq c_{i,j} \geq 0, \quad i = 1, \ldots, m, \quad j = \tilde{t}_f^i, \ldots, n_i - 2. \quad (3)$$

If we assume that each training unit is equally important, then the following constraint must be satisfied:

$$\sum_{j=\tilde{t}_f^i}^{n_i-1} c_{i,j} = 1, \quad i = 1, \ldots, m. \tag{4}$$

We can assume $\{c_{i,j}\}$ follows an arithmetic series ($2c_{i,j} = c_{i,j+1} + c_{i,j-1}$) or a geometric series ($c_{i,j}^2 = c_{i,j+1}c_{i,j-1}$) depending on the emphasis placed on the monotonicity. As a result, $c_{i,j}$ can be computed by initializing $c_{i,\tilde{t}_f^i}$ to be a small positive number and using one of the following expressions depending on which assumption is chosen.

— For an arithmetic series

$$c_{i,j} = c_{i,\tilde{t}_f^i} + \left(j - \tilde{t}_f^i\right) \frac{2 - 2c_{i,\tilde{t}_f^i}\left(n_i - \tilde{t}_f^i\right)}{\left(n_i - \tilde{t}_f^i\right)\left(n_i - \tilde{t}_f^i - 1\right)}, \quad j = \tilde{t}_f^i, \ldots, n_i - 1. \tag{5}$$

— For a geometric series

$$c_{i,j} = c_{i,\tilde{t}_f^i} * q^{j - \tilde{t}_f^i}, \quad j = \tilde{t}_f^i, \ldots, n_i - 1, \tag{6}$$

where q statisfies $c_{i,\tilde{t}_f^i} q^{n_i - \tilde{t}_f^i} - q + 1 - c_{i,\tilde{t}_f^i} = 0$.

Since more weights will be assigned to $\varepsilon_{i,j}$ as j increases, the estimated vector of weight coefficients, $\boldsymbol{w}$, becomes progressively dominated by the sensor data at observation epochs that are closer to the failure point. We will show in the case study section that our composite health index has the advantage that it will be robust with respect to the uncertainties in estimating the incipient fault time.

4) Selection of Data-Fusion Function: The formulation expressed in (2) uses a weighted average data-fusion function to combine the selected sensor data (i.e., $\boldsymbol{w}'\boldsymbol{M}'\boldsymbol{1} = 1$). The vector $\boldsymbol{w}$ measures the relative importance of each sensor, and thus the composite health index is a weighted average of the sensor data. It is worth noting that the linearity assumption may not be suitable in some applications, in which case nonlinear functions may be used when developing the health index.

5) Tuning Parameter Setting: The tuning parameter r is used to control the relative importance given the two terms of the objective function, monotonicity and threshold variance, in (2). The optimal value of r can be obtained by cross-validation. For K-fold cross-validation, we can split the training data into K equal-sized groups. For a particular value of $r (0 < r < 1)$, we leave the kth group data out and train the model in (2) based on the $K - 1$ groups of data. Next, we calculate the amount of violation in the monotonic property, VM_k and the variance in the failure threshold, VF_k. We repeat the procedure for $k = 1, \ldots, K$ and combine VM_k and VF_k for different k (e.g., $\mathrm{VM} = \sum_{k=1}^{K} \mathrm{VM}_k/K$, $\mathrm{VF} = \sum_{k=1}^{K} \mathrm{VF}_k/K$) and use it as the evaluation criterion for the chosen r value. Clearly, increasing r puts more emphasis on reducing the variance in the failure threshold on the expense of increasing the possibility of violating the monotonic property of the health index.

To solve a multiobjective optimization problem, one standard approach is to plot the efficient frontier with respect to the two terms of the objective function in (2). It is known that when moving from one solution to another on the efficient frontier, there is always a certain amount of sacrifice in one objective (e.g., increased amount of violation in the monotonic property), in order to achieve a certain amount of gain in the other (e.g., decreased variance in the failure threshold). In practice, the optimal value of r depends on the different emphasis we place on the two terms of the objective function.

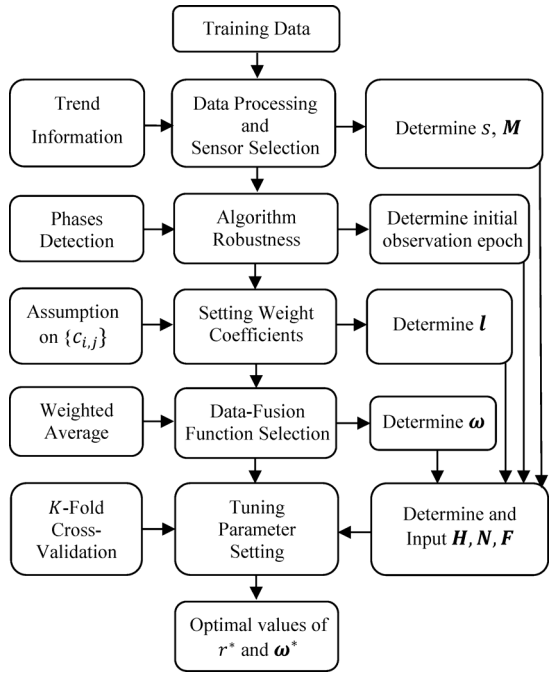

Fig. 5. Flow chart of the proposed data-level fusion approach.

D. Flow Chart of the Data-Level Fusion Approach

Fig. 5 illustrates the flow chart of our proposed data-level fusion approach based on multiple sensor data for degradation modeling and prognostics. Denote the optimal values of r and $\boldsymbol{\omega}$ as r^* and $\boldsymbol{\omega}^*$. Only the first s entries of $\boldsymbol{\omega}^*$, which are the optimal values of $\boldsymbol{w}$, $\boldsymbol{w}^*$, will be used to construct the health index for testing units.

IV. Case Study

In this case study, we investigate the performance of our data-level fusion methodology using degradation-based sensor data pertaining to turbofan engines. The dataset consists of 100 training units (i.e., $m = 100$) with a total of 20 631 observation epochs (i.e., $\sum_{i=1}^{m} n_i = 20\,631$), 100 testing units with a total of 13 096 observation epochs, and a file recording the actual remaining lifetime of the 100 testing units. (Additional details pertaining to the experimental setup and simulation model used to generate the data have been discussed earlier in Section II.) Detailed procedures for data processing and sensor selection, algorithm robustness, weight coefficients setting, data-fusion function selection, tuning parameter setting, and computational complexity analysis are illustrated in this section.

To numerically evaluate the improved performance of the composite health index when it is used for model fitting and remaining life prediction, the stochastic degradation modeling framework [4] is adopted to compute and update the remaining life distribution (RLD) of each unit in real-time. We will compare the accuracy of predictions using the composite health

index and that resulting from using each individual sensor based on the same stochastic degradation modeling framework [4]. It is worth mentioning that the composite health index can be considered as another sensor data, which can be directly treated as an input for other feature-level or decision level fusion methods. Since the input data become more informative, the accuracy of predictions is expected to be improved by using both the composite health index and the original sensor data.

A. Data Processing and Selection

Among the 21 outputs listed in Table I, 11 sensor data are selected. The selection is made on the basis that the data shows a consistent degradation trend for all training units. Those 11 (i.e., $s = 11$) sensors are T24, T50, P30, Nf, Ps30, phi, NRf, BPR, htBleed, W31 and W32. Furthermore, the corresponding diagonal elements of $\boldsymbol{M}$ are identified as $[1, 1, -1, 1, 1, -1, 1, 1, 1, -1, -1]'$. Recall that 1 refers to an increasing trend, while -1 refers to a decreasing trend.

B. Algorithm Robustness

As mentioned before, since more weights will be assigned to $\varepsilon_{i,j}$ as j increases, the estimated vector of weight coefficients, $\boldsymbol{w}$, becomes progressively dominated by the sensor data at observation epochs that are closer to the failure point. To demonstrate this point, we consider the constraint: $n_i - \tilde{t}_f^i = p, \forall i$, where p represents the number of observation epochs in the defective phase. This constraint ensures that the number of observations (from the defective phase) used to construct the health index is the same for all training units. Since each unit has different values for n_i and $\tilde{t}_f^i$, there are no guarantees that the defective phases of all the training units will be equal to p. In what follows, we will show that even when last p observations before failure are used, the methodology still provides a reasonably robust estimation of the weight vector.

Fig. 6 illustrates the relationship between the estimated optimal weights $\boldsymbol{w}^*$ and different values of p. It is clear from the graph that beyond specific values for p, the estimated $\boldsymbol{w}^*$ becomes relatively unaffected by changes of p. Furthermore, as p increases, the elements of $\boldsymbol{w}^*$ converge to constant values. Based on our experimental observations, as shown in Fig. 6, we use the last 100 observations (i.e., $p = 100$) of each unit when estimating $\boldsymbol{w}^*$ in (1).

In addition, a discrete random number has been added to $p = 100$ to simulate the estimation uncertainties of the defective phase in each unit. The experiments yield similar robust result, where $\boldsymbol{w}^*$ is also robust with respect to the uncertainties in estimating the defective phase in each unit. Results have been omitted due to the page limit restrictions. Thus, as long as sufficient observation epochs are selected to represent the defective phase (i.e., p is sufficiently large), $\boldsymbol{w}^*$ will be relatively robust.

C. Setting Weight Coefficients and Selecting the Data-Fusion Function

An arithmetic series for $\{c_{i,j}\}$ is adopted by assuming linearly increasing weight coefficients. Recall that these coefficients capture the violation in the monotonic property as unit i degrades. In addition, a weighted average data-fusion function is selected for demonstration.

TABLE II
OPTIMAL WEIGHTS $\boldsymbol{w}^*$ TO COMBINE THE SELECTED SENSOR DATA

Name	T24	T50	P30	Nf	Ps30	phi
Value	0.0568	0.1081	-0.0994	0.1021	0.1488	-0.1226
Name	NRf	BPR	htBleed	W31	W32	
Value	0.1030	0.0726	0.0526	-0.0649	-0.0691	

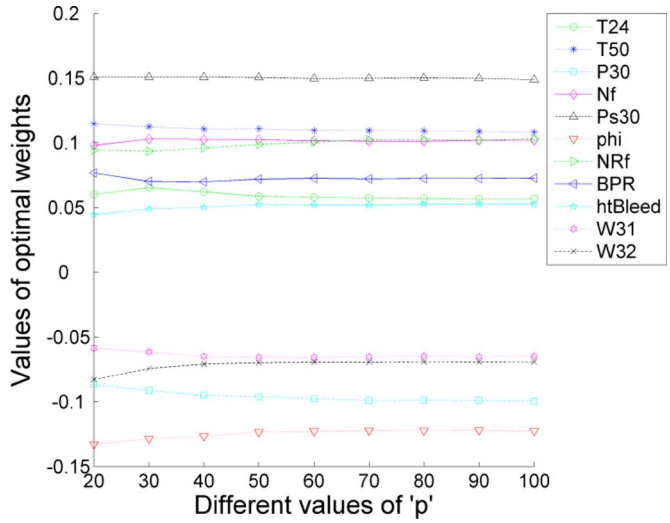

Fig. 6. Changes in the optimal weights $\boldsymbol{w}^*$ at different values of p.

D. Tuning Parameter Setting

As mentioned earlier, the optimal value of the tuning parameter, r^*, can be estimated using K-fold cross-validation. For the purpose of this study, K is chosen to be 5. Thus, in each fold validation, we train the model in (2) using 80 training units. For each selected r value, we calculate the average amount of violation in monotonicity, VM, and the average variance of the failure threshold, VF, of the composite health index using five-fold cross-validation.

Fig. 7 plots the relationship between the amount of violation in monotonicity versus the variance in the failure threshold for different r values. This efficient frontier plot demonstrates that as r becomes larger, the amount of violation in monotonicity trend increases and the variance in the failure threshold decreases.

In this case study, we choose $r = 0.4$ because the marginal reduction in the violation in monotonicity is small compared to the marginal increase in the variance of the failure threshold. In practice, the value of r can be chosen depending on how important each property is when developing the composite health index. Setting $r = 0.4$ and solving the quadratic formulation in (2) for the selected sensor data, we get the optimal weights $\boldsymbol{w}^*$, which are summarized in Table II.

E. Computational Complexity Analysis

All numerical experiments are performed using MATLAB V7.9 and TOMLAB V7.8 [27] in Windows 7 operating system with two Intel Core i7-2820QM 2.30 GHz processors and 8 GB RAM. Most of the computational time was used for solving the optimization model expressed in (2) with $s + \sum_{i=1}^{80}(n_i - \tilde{t}_f^i) = 11 + 80 * 100 = 8011$ number of variables and $s + 2 * \sum_{i=1}^{80}(n_i -$

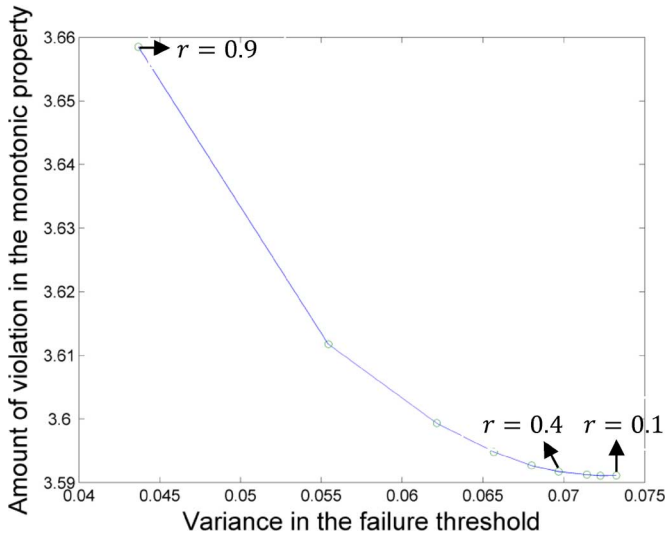

Fig. 7. Efficient frontier of the amount of violation in the monotonic property V.S. the variance in the failure threshold of the health index.

$\tilde{t}_f^i) = 16011$ number of inequality constraints. Our experimental study shows that on average it takes about 6 s to solve the optimization problem using CPLEX solver in Tomlab [27].

F. Stochastic Degradation Modeling With Exponential Function Form

1) Degradation Model Development: Based on the scatter plot of the sensor data in Fig. 8, degradation signals show exponential functional forms. The exponential functional form has been widely used to model cumulative damage processes [4], [21], [28]. In this case study, we use the stochastic degradation modeling approach proposed in [4] to evaluate the performance of the composite health index when used to predict remaining lifetime.

We begin by assuming that the sensor data $x_{i,k,j}$ satisfies

$$x_{i,k,j} = \phi_k + \theta_{i,k} e^{\alpha_{i,k} * j + \beta_{i,k} * j^2 + \tau_{i,k}(j) - \frac{\sigma_k^2}{2}} \tag{7}$$

where ϕ_k is a constant deterministic parameter for sensor k, $\theta_{i,k}$, $\alpha_{i,k}$ and $\beta_{i,k}$ are random variables, and $\tau_{i,k}(j)$ is normally distributed random error term with mean 0 and variance σ_k^2. Since $E(e^{\tau_{i,k}(j) - (\sigma_k^2)/(2)}) = 1$, then $E(x_{i,k,j} \,|\, \theta_{i,k}, \alpha_{i,k}, \beta_{i,k}) = \phi_k + \theta_{i,k} e^{\alpha_{i,k} * j + \beta_{i,k} * j^2}$. Similar to the work presented in [4] we use the log transformation, i.e., we define $L_{i,k,j}$ as

$$L_{i,k,j} = \ln(x_{i,k,j} - \phi_k) = \theta'_{i,k} + \alpha_{i,k} * j + \beta_{i,k} * j^2 + \tau_{i,k}(j) \tag{8}$$

where $\theta'_{i,k} = \ln \theta_{i,k} - (\sigma_k^2)/(2)$. We further assume that the stochastic parameters $\theta'_{i,k}$, $\alpha_{i,k}$ and $\beta_{i,k}$ are jointly distributed and follow a multivariate normal distribution:

$$\boldsymbol{\Gamma_{i,k}} = \begin{pmatrix} \theta'_{i,k} \\ \alpha_{i,k} \\ \beta_{i,k} \end{pmatrix} \sim N_3 \left(\boldsymbol{u_0^k}, \boldsymbol{\Sigma_0^k} \right).$$

2) Parameter Estimation: The prior distribution of the $\boldsymbol{\Gamma_{i,k}}$ can be estimated by fitting the degradation path of each training unit with the model defined in (8). σ_k^2 can be estimated by using the residual sum of square over the total number of degree of freedom in the training stage. Once the prior joint distribution of the stochastic parameters is estimated, it is updated using sensor data obtained from each individual testing unit. Next, the updated degradation model can be utilized to compute the RLD which is particular to this testing unit. This process emulates the utilization of in-situ sensor signals to update the remaining lifetime estimation based on the unique degradation characteristics of each unit.

Fig. 8 shows the result of fitting the exponential model to each selected sensor data, and to the composite health index obtained for a random training unit. Table III summarizes the estimated σ_k^2 for all selected sensors and the health index. It clearly shows that the composite health index gives a much better fitting result.

Let $\boldsymbol{L_{.,k,n_.}}$ be the sequence of the log transformed data, which records the last observations before failure in all training units for sensor k, and $\boldsymbol{L_{.,k,n_.}} = [L_{1,k,n_1}, \ldots, L_{m,k,n_m}]'$. Denote the mean of failure threshold for sensor k as u_d^k and the variance of failure threshold for sensor k as v_d^k. u_d^k and v_d^k can be estimated by calculating the mean and the variance of $\boldsymbol{L_{.,k,n_.}}$, respectively. Table IV summarizes the variance of the failure threshold for all selected sensors and the health index, respectively. It clearly shows that variance of the failure threshold in the composite health index is much smaller than the one in any other sensor data due to the formulation in (2).

3) Estimation of Updated Residual Life Distribution: Let $\boldsymbol{L_{i,k,.}}$ be the sequence of the log transformed data observed up to current observation epoch n_i for unit i and sensor k, such that $\boldsymbol{L_{i,k,.}} = [L_{i,k,1}, \ldots, L_{i,k,n_i}]'$. The posterior distribution of $\boldsymbol{\Gamma_{i,k}}$ still follows a multivariate normal distribution: $\boldsymbol{\Gamma_{i,k}} | \boldsymbol{L_{i,k,.}} \sim N_3(\boldsymbol{u_p^{i,k}}, \boldsymbol{\Sigma_p^{i,k}})$, where

$$\boldsymbol{u_p^{i,k}} = \left(\frac{\boldsymbol{\Psi_i' \Psi_i}}{\sigma_k^2} + \left(\boldsymbol{\Sigma_0^k} \right)^{-1} \right)^{-1} \left(\frac{\boldsymbol{\Psi_i' L_{i,k,.}}}{\sigma_k^2} + \left(\boldsymbol{\Sigma_0^k} \right)^{-1} \boldsymbol{u_0^k} \right),$$

$$\boldsymbol{\Sigma_p^{i,k}} = \left(\frac{\boldsymbol{\Psi_i' \Psi_i}}{\sigma_k^2} + (\boldsymbol{\Sigma_0^k})^{-1} \right)^{-1} \quad \text{and}$$

$$\boldsymbol{\Psi_i} \in R^{n_i \times 3} = \begin{bmatrix} 1 & 1 & 1 \\ \ldots & \ldots & \ldots \\ 1 & j & j^2 \\ \ldots & \ldots & \ldots \\ 1 & n_i & n_i^2 \end{bmatrix}$$

(see Appendix C for details).

Define $\tilde{T}_{i,k}$ as the estimated remaining lifetime of testing unit i based on the signal from sensor k. We are interested in deriving the RLD by evaluating the distribution of the time at which the sensor signal crosses the failure threshold. Since $L_{i,k,n_i+t} = \theta'_{i,k} + \alpha_{i,k} * (n_i + t) + \beta_{i,k} * (n_i + t)^2 + \tau_{i,k}(n_i + t)$, then L_{i,k,n_i+t} is normally distributed with mean $\tilde{u}_{i,k,n_i+t}$ and variance $\tilde{\sigma}^2_{i,k,n_i+t}$, where $\tilde{u}_{i,k,n_i+t} = [1, n_i + t, (n_i + t)^2] \boldsymbol{u_p^{i,k}}$ and $\tilde{\sigma}^2_{i,k,n_i+t} = [1, n_i + t, (n_i + t)^2] \boldsymbol{\Sigma_p^{i,k}} [1, n_i + t, (n_i + t)^2]' + \sigma_k^2$. Further, we assume that the failure thresholds for different units are independent. Thus, the conditional cumulative distribution

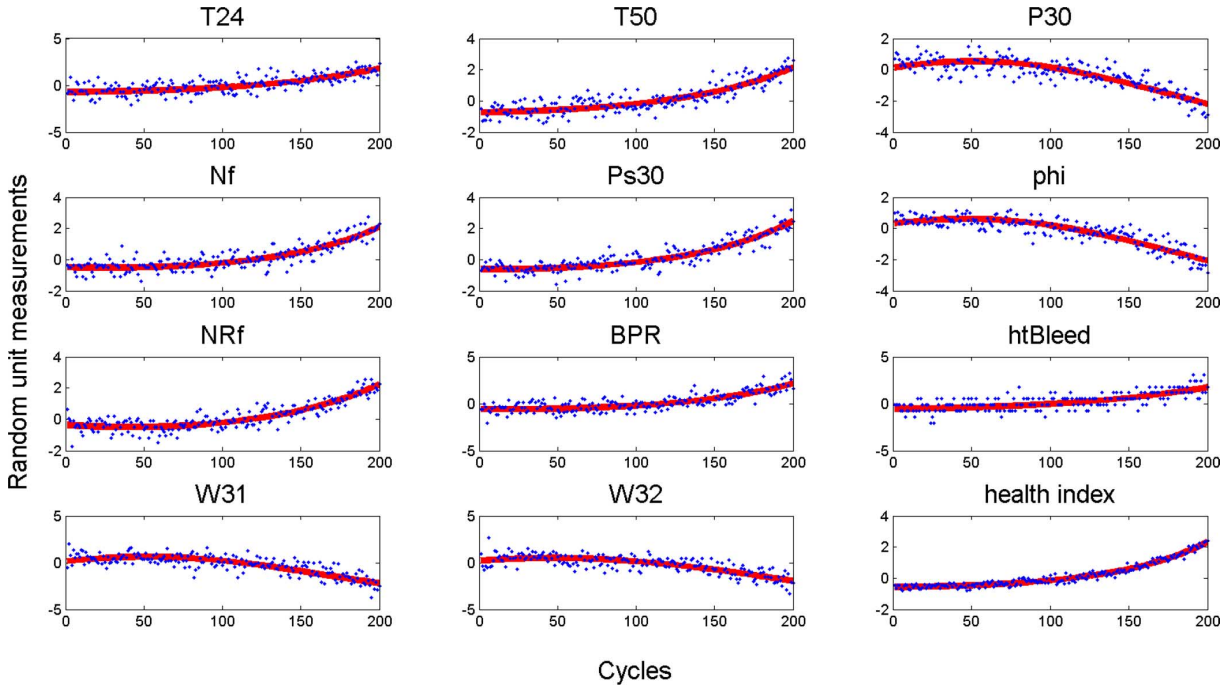

Fig. 8. Degradation signals plot and model fittings for all selected sensor data and the health index in training unit #1.

TABLE III
ESTIMATED σ_k^2 OF ALL SELECTED SENSORS AND THE HEALTH INDEX

Name	T24	T50	P30	Nf	Ps30	phi
Value	0.0795	0.067	0.0676	0.0634	0.0574	0.0591
Name	NRf	BPR	htBleed	W31	W32	health index
Value	0.0615	0.0751	0.1052	0.081	0.0789	0.0189

TABLE IV
VARIANCE IN THE FAILURE THRESHOLD OF ALL SELECTED SENSORS AND THE HEALTH INDEX

Name	T24	T50	P30	Nf	Ps30	Phi
Var.	0.0274	0.0140	0.0264	0.0683	0.0154	0.0206
Name	NRf	BPR	htBleed	W31	W32	health index
Var.	0.0580	0.0225	0.0435	0.0220	0.0317	0.0101

function (cdf) of the estimated remaining lifetime $\tilde{T}_{i,k}$ given the historical data $\boldsymbol{L_{i,k}}_{,.}$ is

$$\begin{aligned} F_{\tilde{T}_{i,k}|\boldsymbol{L_{i,k}}_{,.}}(t) &= P(\tilde{T}_{i,k} \le t|\boldsymbol{L_{i,k}}_{,.}) \\ &= P\left(L_{i,k,n_i+t} \ge u_d^k|\boldsymbol{L_{i,k}}_{,.}\right) \\ &= 1 - P\left(L_{i,k,n_i+t} < u_d^k|\boldsymbol{L_{i,k}}_{,.}\right) \\ &= \Phi\left(\frac{u_d^k - \tilde{u}_{i,k,n_i+t}}{\sqrt{\tilde{\sigma}^2_{i,k,n_i+t} + v_d^k}}\right) = \Phi(g(t)) \end{aligned} \tag{9}$$

where $\Phi(\cdot)$ is the cdf of the standard normal distribution. Conditional on the fact that $\tilde{T}_{i,k} \ge 0$, the truncated cdf for $\tilde{T}_{i,k}$ can be written as

$$\begin{aligned} P(\tilde{T}_{i,k} \le t|\boldsymbol{L_{i,k}}_{,.}, T_{i,k} \ge 0) &= \frac{P(0 \le \tilde{T}_{i,k} \le t|\boldsymbol{L_{i,k}}_{,.})}{P(\tilde{T}_{i,k} \ge 0|\boldsymbol{L_{i,k}}_{,.})} \\ &= \frac{\Phi(g(t)) - \Phi(g(0))}{1 - \Phi(g(0))}. \end{aligned} \tag{10}$$

Since the RLD is skewed, it is preferable to utilize the median as the point estimator of the remaining lifetime. Numerically, this can be estimated by finding the observation epoch t where $P(\tilde{T}_{i,k} \le t|\boldsymbol{L_{i,k}}_{,.}, \tilde{T}_{i,k} \ge 0) = 0.5$.

Fig. 9 illustrates the original and the updated degradation model of a random testing unit in all selected sensors and the health index. The solid line shows the original model fitting based on the priors which are estimated from training units, whereas the dashed line presents the updated model fitting based on the collected sensor data for this particular testing unit. Similar to Fig. 8, the composite health index shows a much better monotonic property and model fitting result.

G. Prediction Results

To evaluate the performance of the health index for remaining life prediction, we compute the percentage difference between the predicted and the actual failure time. We consider two cases for the predicted failure time: 1) when it is estimated based on the composite health index and 2) when it is estimated based on each individual sensor signal. Specifically, we define the percentage error, $\text{err}_{i,k}$, as the relative difference between the predicted and the actual failure time for unit i and sensor k, which is expressed as

$$\text{err}_{i,k} = \frac{(n_i + \tilde{T}_{i,k}) - (n_i + T_i)}{n_i + T_i} = \frac{\tilde{T}_{i,k} - T_i}{n_i + T_i} \tag{11}$$

where n_i is the number of available observation epochs of testing unit i when it stops further usage; T_i is the actual remaining lifetime for unit i and $\tilde{T}_{i,k}$ is the estimated remaining lifetime for unit i and sensor k.

Since different testing units stop further usage at different time, we compare the absolute value of the mean percentage error by using each selected sensor and the composite health index at different levels of actual remaining lifetime, as shown

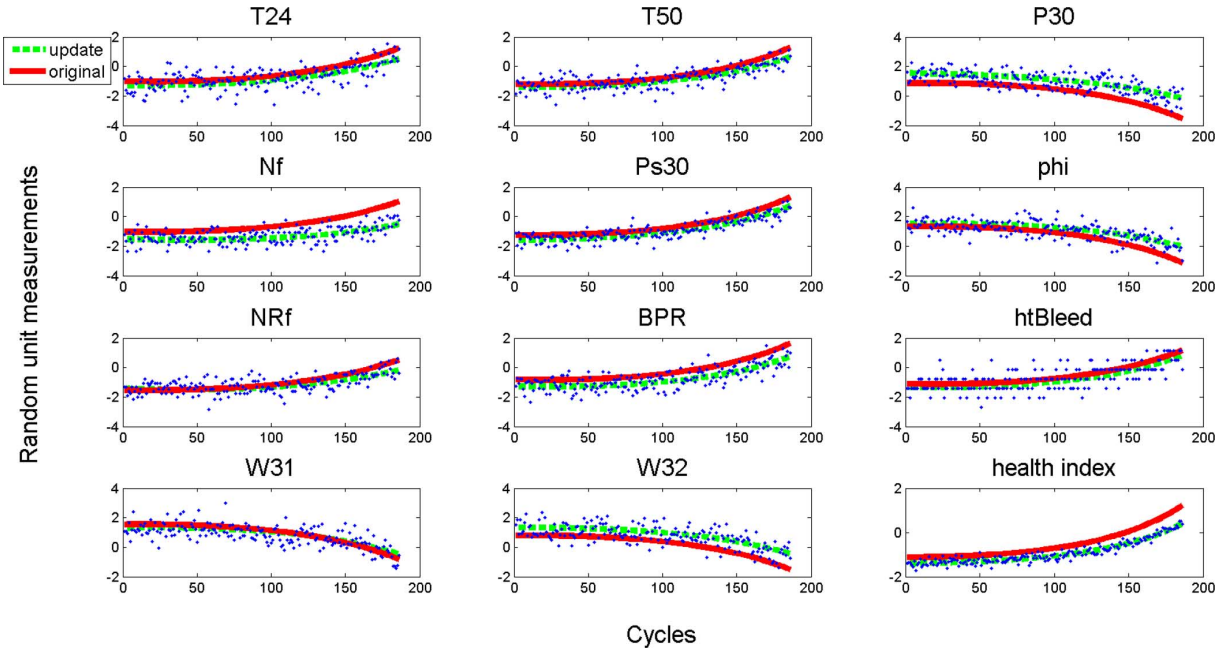

Fig. 9. Degradation signals plot with original and updated model fitting for all selected sensor data and the health index in testing unit #24.

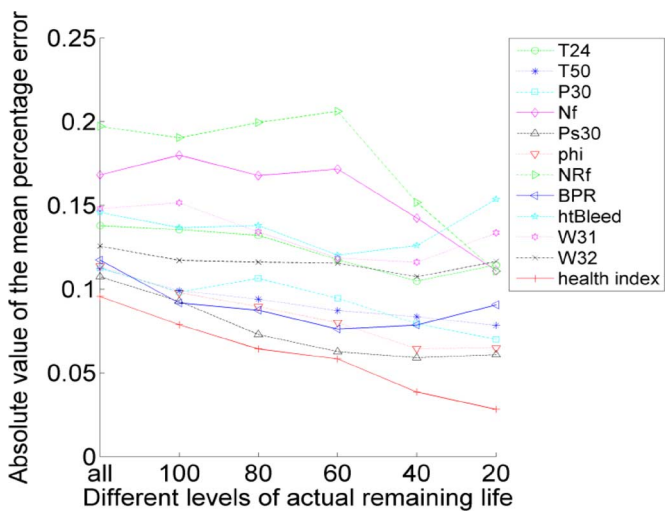

Fig. 10. Comparison results of the absolute value of the mean percentage error by using each selected sensor and the health index at different levels of the actual remaining lifetime.

in Fig. 10. For example, the points correspond to the "all" label are the comparison results based on all 100 testing units whereas the points correspond to the "80" label are the comparison results based on the testing units with equal to or less than 80 actual remaining observation epochs.

Using the results in Fig. 10, we can make the following observations.

i) The composite health index outperforms any single sensor data when it is used for remaining life prediction, which results from the controls on two terms in (2) when developing the composite health index: maximizing the monotonic property and minimizing the variance in the failure threshold.

ii) The advantages of the composite health index for remaining life prediction become more obvious when the unit approaches the actual failure time. For example, at label "40" or "20," the percentage error of remaining life prediction by using the composite health index is much smaller than the one by using any other sensor data. The first reason for this phenomenon is that as the actual remaining lifetime becomes smaller, our predictions are made for a shorter future time period, and therefore less uncertainty is involved. Second, less actual remaining lifetime usually indicates more historical data have been collected, and thus we are more confident about the updated fitting models. The final possible explanation is since we assign higher weights to the slack variables, $\varepsilon_{i,j}$ as j increases, the remaining life prediction by using the composite health index becomes more accurate when we make the prediction at the observation epoch that is closer to the actual failure time. This unique characteristic of the composite health index has significant practical impact, especially with regards to safety.

Often practitioners are not only interested in point estimation of the remaining lifetime, but also interested in evaluating a confidence interval (CI) of the predicted remaining lifetime. Confidence intervals can be obtained by the truncated cdf of the estimated remaining lifetime $\tilde{T}_{i,k}$ in (10). Fig. 11 shows the 95% CIs of the remaining life prediction for testing unit #24 for each selected sensor as well as the composite health index. The bars represent the 95% CIs of the remaining life prediction, and the dots represent the point estimates. The dashed horizontal line represents the actual value of the remaining lifetime.

It is clear that using the composite health index to predict the remaining lifetime provides the narrowest CI. Due to the goodness of model fitting and low variance of the failure threshold, the denominator in the $\Phi(\cdot)$ operation of (9) by using the composite health index is smaller than the one by

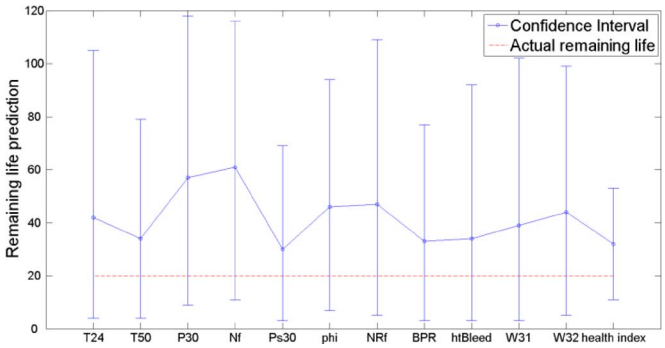

Fig. 11. Confidence intervals of the remaining life prediction for the testing unit #24 by using each selected sensor and the health index.

TABLE V
MEAN WIDTHS OF THE 95% CIS OF THE REMAINING LIFE PREDICTION IN ALL TESTING UNITS USING ALL SELECTED SENSORS AND THE HEALTH INDEX

Name	T24	T50	P30	Nf	Ps30	phi
Width	195.8	168.6	178.7	195.2	160.03	157.0
Name	NRf	BPR	htBleed	W31	W32	health index
Width	190.0	183.7	212.3	202.8	190.4	98.2

using any other sensor data, which results in the narrowest CI in the health index. Table V summarizes the mean of the widths of the 95% CIs of the remaining life predictions for all testing units when evaluated using each selected sensor versus the composite health index. According to the results of Table V, using the composite health index for remaining life prediction can reduce the widths of the 95% CIs by 37.5% (i.e., (157.0–98.2)/157.0). Thus, the composite health index can provide a more precise estimation of the remaining lifetime.

V. DISCUSSION AND CONCLUSION

This paper develops a systematic approach which includes data selection, data processing, and data fusion steps that lead to an improved degradation-based prognostic model. The novelty of this methodology lies in the development of a data-level fusion technique that combines signals from multiple sensors. By identifying the two essential properties that degradation signals should have for successful prognostic applications (i.e., maximizing the monotonic property and minimizing the variance in the failure threshold), a composite health index can be developed to better characterize the degradation performance of each system. Guidelines for several key elements related to the problem formulation, algorithm robustness, weight coefficients setting, selection of data-fusion function, and other important aspects are discussed and illustrated in the case study. One advantage of this methodology is that the remaining life prediction becomes more accurate as the unit approaches failure compared with using each individual sensor. This property could have a great impact on deciding when to schedule maintenance or to stop operation in practice. Another advantage of this methodology is that the widths of the CI can be significantly reduced by using the composite health index for remaining life prediction, which indicates the composite health index can be a more efficient tool for prognostics.

The methodology was tested and validated using the degradation sensor data of aircraft gas turbine engine that were generated by C-MAPSS [16]. The stochastic degradation modeling framework [4] was adopted to numerically evaluate the performance of the composite health index by computing and updating the RLD of each unit in real-time. However, the methodology developed in this paper is not limited to this type of modeling framework. In other words, the composite health index can be considered as another sensor data, which can be directly treated as an input for other feature-level or decision level fusion methods. Since the input data become more informative, the accuracy of predictions is expected to be improved by using both the composite health index and the original sensor data.

This research establishes a new direction in data fusion by proposing an appropriate data-level fusion technique that is specifically beneficial for degradation modeling and prognostic applications. There are several important topics for future research that are related to this work. First, further studies can be done to investigate the performance when nonlinear features are created and the kernel methods are used to map *in-situ* sensor data into higher dimensional space. Second, although this paper focuses on the degradation dataset with a single operation condition and a single failure mode, extensions to the cases that have more than one failure mode or operational condition are worthy of further exploration.

APPENDIX A

This appendix shows that the variance in the failure threshold of the composite health index can be expressed as the quadratic term: $\boldsymbol{w'Y'DYw}$. The unbiased sample variance can be estimated by: $((\boldsymbol{Yw})'(\boldsymbol{Yw}) - m((\boldsymbol{1'Yw})/(m))^2)/(m-1) = (\boldsymbol{w'Y'Yw} - (\boldsymbol{w'Y'11'Yw})/m)/(m-1) = \boldsymbol{w'Y'}((\boldsymbol{I}-(\boldsymbol{11'})/m)/(m-1))\boldsymbol{Yw} = \boldsymbol{w'Y'DYw}$.

APPENDIX B

This appendix proves that $\boldsymbol{H}$ is positive semidefinite (P.S.D) matrix. First, it is straightforward to show that $\boldsymbol{D} = (\boldsymbol{I} - \boldsymbol{O}/m)/(m-1)$ is a symmetric P.S.D matrix. Then, $\boldsymbol{D}$ can be decomposed as: $\boldsymbol{D} = \boldsymbol{LL'}$ by Cholesky decomposition, where $\boldsymbol{L}$ is a lower triangular matrix. Next, $\boldsymbol{H}$ can be written as: $\boldsymbol{H} = \boldsymbol{G'Y'DYG} = (\boldsymbol{L'YG})'\boldsymbol{L'YG}$. Thus, $\boldsymbol{H}$ is P.S.D.

APPENDIX C

This appendix derives the posterior distribution of $\boldsymbol{\Gamma_{i,k}}$ still follows a multivariate normal distribution with mean $\boldsymbol{u_p^{i,k}} = ((\boldsymbol{\Psi_i'\Psi_i})/(\sigma_k^2) + (\boldsymbol{\Sigma_0^k})^{-1})^{-1}((\boldsymbol{\Psi_i'L_{i,k,.}})/(\sigma_k^2) + (\boldsymbol{\Sigma_0^k})^{-1}\boldsymbol{u_0^k})$ and variance $\boldsymbol{\Sigma_p^{i,k}} = ((\boldsymbol{\Psi_i'\Psi_i})/(\sigma_k^2) + (\boldsymbol{\Sigma_0^k})^{-1})^{-1}$. The multivariate normal distribution can be expressed as $P(\boldsymbol{\Gamma_{i,k}}) = (1)/((2\pi)^{3/2}|\boldsymbol{\Sigma_0^k}|^{1/2})e^{-(1)/(2)(\boldsymbol{\Gamma_{i,k}}-\boldsymbol{u_0^k})'(\boldsymbol{\Sigma_0^k})^{-1}(\boldsymbol{\Gamma_{i,k}}-\boldsymbol{u_0^k})}$. Thus

$$\begin{aligned} P(\boldsymbol{\Gamma_{i,k}}|\boldsymbol{L_{i,k,.}}) &\propto P(\boldsymbol{L_{i,k,.}}|\boldsymbol{\Gamma_{i,k}})P(\boldsymbol{\Gamma_{i,k}}) \\ &\propto e^{-\frac{1}{2\sigma_k^2}(\boldsymbol{L_{i,k,.}}-\boldsymbol{\Psi_i\Gamma_{i,k}})'(\boldsymbol{L_{i,k,.}}-\boldsymbol{\Psi_i\Gamma_{i,k}})} \\ &\quad \times e^{-\frac{1}{2}(\boldsymbol{\Gamma_{i,k}}-\boldsymbol{u_0^k})'(\boldsymbol{\Sigma_0^k})^{-1}(\boldsymbol{\Gamma_{i,k}}-\boldsymbol{u_0^k})} \\ &\propto e^{\boldsymbol{\Gamma'_{i,k}}(\frac{\boldsymbol{\Psi_i'\Psi_i}}{\sigma_k^2}+(\boldsymbol{\Sigma_0^k})^{-1})\boldsymbol{\Gamma_{i,k}}-2(\frac{\boldsymbol{L'_{i,k,.}\Psi_i}}{\sigma_k^2}+(\boldsymbol{u_0^k})'(\boldsymbol{\Sigma_0^k})^{-1})\boldsymbol{\Gamma_{i,k}}} \end{aligned} \quad (12)$$

It is known that if $P(\boldsymbol{L_{i,k,.}}|\boldsymbol{\Gamma_{i,k}})$ follows normal distribution and $P(\boldsymbol{\Gamma_{i,k}})$ follows multivariate normal distribution, the posterior will also follow multivariate normal distributions. As a result, $\boldsymbol{\Gamma_{i,k}}|\boldsymbol{L_{i,k,.}} \sim N_3(\boldsymbol{u_p^{i,k}}, \boldsymbol{\Sigma_p^{i,k}})$ and $P(\boldsymbol{\Gamma_{i,k}}|\boldsymbol{L_{i,k,.}}) \propto e^{-(1)/(2)(\boldsymbol{\Gamma_{i,k}}-\boldsymbol{u_p^{i,k}})'(\boldsymbol{\Sigma_p^{i,k}})^{-1}(\boldsymbol{\Gamma_{i,k}}-\boldsymbol{u_p^{i,k}})}$.

Comparing (12) with $(\boldsymbol{\Gamma_{i,k}} - \boldsymbol{u_p^{i,k}})'(\boldsymbol{\Sigma_p^{i,k}})^{-1}(\boldsymbol{\Gamma_{i,k}} - \boldsymbol{u_p^{i,k}}) = \boldsymbol{\Gamma'_{i,k}}(\boldsymbol{\Sigma_p^{i,k}})^{-1}\boldsymbol{\Gamma_{i,k}} - 2(\boldsymbol{u_p^{i,k}})'(\boldsymbol{\Sigma_p^{i,k}})^{-1}\boldsymbol{\Gamma_{i,k}} + (\boldsymbol{u_p^{i,k}})'(\boldsymbol{\Sigma_p^{i,k}})^{-1}\boldsymbol{u_p^{i,k}}$, we get the equations $(\boldsymbol{\Sigma_p^{i,k}})^{-1} = ((\boldsymbol{\Psi_i'\Psi_i})/(\sigma_k^2) + (\boldsymbol{\Sigma_0^k})^{-1})$ and $(\boldsymbol{u_p^{i,k}})'(\boldsymbol{\Sigma_p^{i,k}})^{-1} = ((\boldsymbol{L'_{i,k,.}\Psi_i})/(\sigma_k^2) + (\boldsymbol{u_0^k})'(\boldsymbol{\Sigma_0^k})^{-1})$. This finishes the proof that $\boldsymbol{\Gamma_{i,k}}|\boldsymbol{L_{i,k,.}} \sim N_3(\boldsymbol{u_p^{i,k}}, \boldsymbol{\Sigma_p^{i,k}})$, where $\boldsymbol{\Sigma_p^{i,k}} = ((\boldsymbol{\Psi_i'\Psi_i})/(\sigma_k^2) + (\boldsymbol{\Sigma_0^k})^{-1})^{-1}$ and $\boldsymbol{u_p^{i,k}} = ((\boldsymbol{\Psi_i'\Psi_i})/(\sigma_k^2) + (\boldsymbol{\Sigma_0^k})^{-1})^{-1}((\boldsymbol{\Psi_i'L_{i,k,.}})/(\sigma_k^2) + (\boldsymbol{\Sigma_0^k})^{-1}\boldsymbol{u_0^k})$.

REFERENCES

[1] R. K. Mobley, *An Introduction to Predictive Maintenance*. Burlington, MA, USA: Elsevier Butterworth-Heinemann, 2002.

[2] W. Q. Meeker and L. A. Escobar, *Statistical Methods for Reliability Data*. New York, NY, USA: Wiley, 1998.

[3] W. Nelson, *Accelerated Testing Statistical Models, Test Plans, and Data Analysis*. New York, NY, USA: Wiley, 1990.

[4] N. Gebraeel, "Sensory-updated residual life distributions for components with exponential degradation patterns," *IEEE Trans. Autom. Sci. Eng.*, vol. 3, pp. 382–393, Oct. 2006.

[5] D. L. Hall and J. Llinas, "An introduction to multisensor data fusion," *Proc. IEEE*, vol. 85, pp. 6–23, Jan. 1997.

[6] A. J. Volponi, T. Brotherton, R. Luppold, and D. L. Simon, *Development of an Information Fusion System for Engine Diagnostics and Health Management*. Cleveland, OH, USA: NASA, Feb. 2004.

[7] T. Heger and M. Pandit, "Optical wear assessment system for grinding tools," *J. Electron. Imag.*, vol. 13, pp. 450–461, Jul. 2004.

[8] D. Simon and D. L. Simon, "Aircraft turbofan engine health estimation using constrained Kalman filtering," *ASME J. Eng. Gas Turbines Power*, vol. 127, pp. 323–328, Apr. 2005.

[9] T. Kobayashi and D. L. Simon, "Hybrid Kalman filter approach for aircraft engine in-flight diagnostics: Sensor fault detection case," *J. Eng. Gas Turbines Power*, vol. 129, no. 3, pp. 746–754, Jul. 2007.

[10] K. Salahshoor, M. Mosallaei, and M. Bayat, "Centralized and decentralized process and sensor fault monitoring using data fusion based on adaptive extended Kalman filter algorithm," *Measurement*, vol. 41, pp. 1059–1076, Mar. 2008.

[11] K. Goebel and P. Bonissone, "Prognostic information fusion for constant load systems," in *Proc. 7th Annu. Conf. Inform. Fusion*, 2005, vol. 2, pp. 1247–1255.

[12] Q. Sun, "Sensor fusion for vehicle health monitoring and degradation detection," in *Proc. 5th Int. Conf. Inform. Fusion*, Annapolis, MD, USA, 2002, pp. 1422–1427.

[13] A. K. S. Jardine, D. Lin, and D. Banjevic, "A review on machinery diagnostics and prognostics implementing condition-based maintenance," *Mechanical Syst. Signal Process.*, vol. 20, no. 7, pp. 1483–1510, 2006.

[14] C. Hu, B. D. Youn, and P. Wang, "Ensemble of data-driven prognostic algorithms with weight optimization and k-fold cross validation," in *Proc. ASME 2010 Int. Design Eng. Tech. Conf. Comput. Inform. Engineering Conf.*, Montreal, Quebec, Canada, 2010, vol. 3, pp. 1023–1032.

[15] C. S. Byington, R. C. Brewer, T. Meyer, and S. R. Amin, "Gearbox corrosion prediction via oil condition sensing and model fusion," in *STLE 62nd Annu. Meeting and Exhibition*, Philadelphia, PA, USA, May 2007, pp. 1–19.

[16] A. Saxena, K. Goebel, D. Simon, and N. Eklund, "Damage propagation modeling for aircraft engine run-to-failure simulation," in *Proc. 1st Int. Conf. Prognostics Health Manage.*, Denver, CO, USA, Oct. 2008, pp. 1–9.

[17] S. Sarkar, X. Jin, and A. Ray, "Data-Driven fault detection in aircraft engines with noisy sensor measurements," *ASME J. Eng. Gas Turbines Power*, vol. 133, p. 081602, Aug. 2011.

[18] D. Frederick, J. DeCastro, and J. Litt, "User's guide for the commercial modular aero-propulsion system simulation (C-MAPSS)," NASA/ARL, Tech. Manual TM2007-215026, 2007.

[19] A. Saxena, J. Celaya, E. Balaban, K. Goebel, B. Saha, S. Saha, and M. Schwabacher, "Metrics for evaluating performance of prognostics techniques," in *Int. Conf. Prognostics and Health Management (PHM08)*, Denver, CO, USA, Oct. 2008, pp. 1–17.

[20] T. Hastie, R. Tibshirani, and J. H. Friedman, *The Elements of Statistical Learning: Data Mining, Inference, and Prediction*. New York, NY, USA: Springer-Verlag, 2003.

[21] N. Gebraeel and M. Lawley, "A neural network degradation model for computing and updating residual life distributions," *IEEE Trans. Autom. Sci. Eng.*, vol. 5, no. 1, pp. 154–163, Jan. 2008.

[22] A. Demetriou and M. M. Polycarpou, "Incipient fault diagnosis of dynamical systems using online approximators," *IEEE Trans. Autom. Control*, vol. 43, no. 11, pp. 1612–1617, Nov. 1998.

[23] M. J. Mousavi and K. L. Butler-Purry, "Detecting incipient faults via numerical modeling and statistical change detection," *IEEE Trans. Power Del.*, vol. 25, pp. 1275–1283, July 2010.

[24] P. M. Frank, "Fault diagnosis in dynamic systems using analytical and knowledge-based redundancy—A survey and some new results," *Automatica*, vol. 26, no. 3, pp. 459–474, May 1990.

[25] X. Zhang, M. M. Polycarpou, and T. Parisini, "A robust detection and isolation scheme for abrupt and incipient faults in nonlinear systems," *IEEE Trans. Autom. Control*, vol. 47, no. 4, pp. 576–593, Apr. 2002.

[26] M. Y. Chow and S. O. Yee, "Methodology for on-line incipient fault detection in single-phase squirrel-cage induction motors using artificial neural networks," *IEEE Trans. Energy Convers.*, vol. 6, pp. 536–545, Sep. 1991.

[27] K. Holmström, A. O. Göran, and M. M. Edvall, *User's Guide for TOMLAB*. San Diego, CA, USA: Tomlab Optimization Inc., Feb. 2008.

[28] N. Gebraeel, "Prognostics-based identification of the top-k units in a fleet," *IEEE Trans. Autom. Sci. Eng.*, vol. 7, no. 1, pp. 37–48, Jan. 2010.

Kaibo Liu received the B.S. degree in industrial engineering and engineering management from the Hong Kong University of Science and Technology, Hong Kong, China, in 2009, and the M.S. degree in statistics from the Georgia Institute of Technology, Atlanta, GA, USA, in 2011. Currently, he is working towards the Ph.D. degree at the H. Milton Stewart School of Industrial and Systems Engineering, Georgia Institute of Technology.

His research interests are focused on data fusion for system modeling, assessment and improvement.

Mr. Liu is a member of ASME, INFORMS, and IIE.

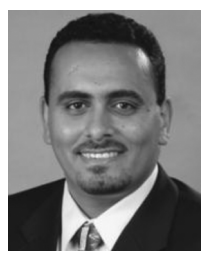

Nagi Gebraeel received the M.S. and Ph.D. degrees in industrial engineering from Purdue University, West Lafayette, IN, USA, in 1998 and 2003, respectively.

Currently, he is an Associate Professor with the H. Milton Stewart School of Industrial and Systems Engineering, Georgia Institute of Technology, Atlanta, GA, USA. His major research interests are in the areas of degradation modeling and sensor-based prognostics, reliability engineering, and maintenance operations and logistics.

Dr. Gebraeel is a member of IIE and INFORMS.

Jianjun Shi received the B.S. and M.S. degrees in electrical engineering from the Beijing Institute of Technology, Beijing, China, in 1984 and 1987, respectively, and the Ph.D. degree in mechanical engineering from the University of Michigan, Ann Arbor, MI, USA, in 1992.

Currently, he is the Carolyn J. Stewart Chair Professor at the H. Milton Stewart School of Industrial and Systems Engineering, Georgia Institute of Technology, Atlanta, GA, USA. His research interests include the fusion of advanced statistical and domain knowledge to develop methodologies for modeling, monitoring, diagnosis, and control for complex manufacturing systems.

Dr. Shi is a Fellow of the IIE, a Fellow of ASME, a Fellow of INFORMS, an elected Member of the ISI, and a Life Member of ASA.